The use of 3D surface fitting for robust polyp detection and classification in CT colonography

Tarik A. Chowdhury, Paul F. Whelan and Ovidiu Ghita

Vision Systems Group, School of Electronic Engineering

Dublin City University, Dublin 9, Ireland

Abstract

In this paper we describe the development of a computationally efficient *computer-aided detection* (CAD) algorithm based on the evaluation of the surface morphology that is employed for the detection of colonic polyps in computed tomography (CT) colonography. Initial polyp candidate voxels were detected using the surface normal intersection values. These candidate voxels were clustered using the normal direction, convexity test, region growing and Gaussian distribution. The local colonic surface was classified as polyp or fold using a feature normalized nearest neighborhood classifier. The main merit of this paper is the methodology applied to select the robust features derived from the colon surface that have a high discriminative power for polyp/fold classification. The devised polyp detection scheme entails a low computational overhead (typically takes 2.20 minute per dataset) and shows 100% sensitivity for phantom polyps greater than 5mm. It also shows 100% sensitivity for

real polyps larger than 10mm and 91.67% sensitivity for polyps between 5 to 10mm with an average of 4.5 false positives per dataset. The experimental data indicates that the proposed CAD polyp detection scheme outperforms other techniques that identify the polyps using features that sample the colon surface curvature especially when applied to low-dose datasets.

Key words:

Polyp detection, CT colonography, feature detection, least square fitting, low-dose.

1 Introduction

Colon cancer is the second leading cause of cancer deaths in the developed nations [1–3]. Early detection and removal of colorectal polyps via screening is the most effective way to reduce colorectal cancer mortality [4–7]. Virtual Colonoscopy (VC) or CT Colonography (CTC) [8–11] is a rapidly evolving technology for the detection of colorectal polyps and permits interactive viewing with two-dimensional (2D) and three-dimensional (3D) image display techniques. This medical imaging method is being widely investigated as a non-invasive examination procedure for the detection of colorectal polyps and many researchers have advocated CTC as the optimal mass screening technique for colorectal cancer [12]. Since the introduction of CTC, a significant number of studies have been conducted to evaluate the performance of *computer aided detection* (CAD) of colonic polyps. In this regard, Vining et al. [13] proposed a method to detect the colonic polyps by analysing the local curvature of the colon surface and they claimed that a 73% sensitivity with 9 to 90 false positives (FP)/dataset was attained. Summers et al. [14,15] developed a method that identifies the convex surfaces that protrude inward from the colon by eval-

2

uating the principle and mean curvature of the colon surface. Their method achieved 29% to 100% sensitivity and 6 to 20 FPs/dataset depending on the filter chosen to evaluate the curvature. Yoshida et al. [16,17] proposed to use of features such as the shape index (cup, rut, saddle, ridge, cap) and curvedness values on small volume of interest and apply fuzzy clustering for polyp detection. They reported 89% sensitivity with 2.0 FP per dataset, but FP per polyp increased by a factor of 1.5 when sensitivity was 100%. Paik et al. [18] proposed a technique based on contour normal intersection to detect surface patches along the colon wall and shows 85% to 90% sensitivity with a high rate of FP. Kiss et al. [19–21] combined the surface normal distribution and sphere fitting to produce 90% polyp sensitivity for polyps higher than 6mm with 2.82 FPs/dataset. Recently, Kiss at el. [22] employed the slope density function to discriminate between polyps and folds and their technique shows 85% sensitivity for polyps higher than 6mm with 2.48 FPs/dataset. More recently, Paik et al. [23] developed a new technique based on surface normal overlap where the sensitivity was 100% with 7.0 FPs/dataset. Acar et al. [24] suggested a method that detects spherical patches by *Hough Transform* (HT) [17] and the algorithm analyses them using the optical flow to decide if they are polyps or not. The sensitivity rate of their method was 100%, specificity was 85% and the level of false positives per dataset was 3. Other interesting automated CAD-CTC techniques include the work of Gokturk et al. [25], Acar et al. [26], Wanga at el. [27], Jerebko et al. [28] and Kiraly et al. [29].

All the above mentioned CAD techniques show different levels of accuracy and indicate that future investigations are needed in order to obtain a robust technique for polyp detection. In this paper, we propose a computationally efficient method for polyp detection based on surface normal concentration,

3

3D histogram and morphological features extracted from the colon surface. The main contribution of this paper is the inclusion of these features that maximize the discrimination between folds and polyps. Also we propose a new approach for data training in order to increase the identification rate for small polyps. The resulting polyp detection algorithm shows a high sensitivity for polyps $> 5mm$ even when applied to low-dose CT datasets.

2 Materials and Method

Prior to their scheduled examination all patients were instructed to take a low-residue diet for 48 hours followed by clear fluids for 24 hours. Prior to the day of examination, patients were prescribed one sachet of Pixcolax at 8.00, a second sachet of Pixcolax at 12.00, a sachet of clean prep in a litre of cold water at 18.00 and a Senokot tablet at 23.00. Before the CT scan, a rectal tube is inserted and the colon is gently insufflated with room air to the maximum level tolerated by the patient. All scans were performed on a commercially available Siemens Somatom multi-slice Spiral CT scanner. The scanning parameters were 120kVp, 100mAs, 2.5x4mm collimation, 3mm slice thickness, 1.5mm reconstruction interval, 0.5s gantry rotation. The scanning time ranges from 20 to 30s, and the image acquisitions were performed in a single breath-hold. The procedure was first performed with the patient in the supine position and then repeated with the patient in the prone position. The number of CT images per scan varies from 200 to 350 depending on the height of the patient. Typically, the size of the volumetric data is approximately 150MB.

3 CAD Algorithm

This paper details the development of a CAD polyp detection technique that evaluates the morphology of the local 3D data. Figure 1 gives an overview of the proposed algorithm, which consists mainly of four steps that are detailed in the following sections of the paper. Sections 3.1 and 3.2 describe the technique used for segmentation and polyp surface generation. Section 4 explains the feature extraction and Section 5 details the adopted classification scheme.

3.1 Segmentation

CT images provide high contrast between the gas and colon surface and the gaseous region can be successfully segmented by applying a standard region growing algorithm [30]. Sometimes remaining residual material and water can create collapses in the colon and the region growing algorithm may require multiple seed points to segment the entire colon. The threshold value for segmentation was set to -800HU, as suggested in [13,31]. The *colonic wall* (CW) is defined as the adjacent voxels having HU values higher than -800HU.

3.2 Polyp Surface Detection

3.2.1 3D Hough Transform

The normal vector for each voxel in the CW-set was calculated using the Zuker and Hummel operator [32]. Each voxel in the CW creates 7 *Hough points* (HP) (see Figure 2) in the normal direction from 2.5mm to 10mm (2.5,

3.75...8.75, 10.0) by varying the parameter t in Eq. 1,

$$p = p_1 + t \times n \qquad (1)$$

where p_1 is the colon wall voxel and n is the normal vector to that voxel. In Eq. 1 the value of t starts from 0.1 and changes at the step size of 0.1mm until all the HP points situated at distances 2.5, 3.75, 5.0, 6.25, 7.5, 8.75, and 10.00mm are generated.

3.2.2 3D Histogram

The HPs are uniformly distributed from 2mm to 10mm along the normal vector direction for each voxel of the colon wall (CW) and the intersections between the HPs are recorded (see Figure 2) in a 3D histogram. Thus, the 3D histogram records the intersections between the HPs that are in fact intersection of the normal vectors. As the normal vectors are determined using 3D local operators their orientation is sensitive to abrupt changes in the 3D structure of the CW, and to reduce the level of noise in the histogram a weighted smoothing procedure is applied using the expression illustrated in Eq. 2,

$$V_{smooth} = \delta \times Voxel + \sum_{0}^{26} \frac{(1 - \delta) \times Voxel_{neighbour}}{26} \qquad (2)$$

where δ is equal to $1/\sqrt{2}$.

3.2.3 Non Maximum Suppression

After smoothing, all $HP's$ having histogram values higher than 4.0 intersections are considered as *initial candidate center points* (ICCP) of the candidate polyp surfaces. Non maximum suppression was applied in the $ICCP$ set to cre-

6

ate potential center points. The cluster of surface points was created by including the *HPs* and their corresponding surface voxels within a certain distance from *ICCP* (10mm to 25mm). It is useful to remember that folds are generally shaped like cylinders and show a uniform distribution of the number of intersections generated by the *HPs* along the axis of the cylinder. Conversely, polyps resemble either spherical or ellipsoidal shapes and show a narrow peak in the 3D histogram. A minimum distance of 10mm was experimentally selected in initial clustering to include the highest possible number of surface points in the clustered surface. The distance threshold varied from 10mm to 25mm depending on the histogram value for each center point in *ICCP*. The candidate surface cluster may include surrounding non-convex surface points or disconnected surfaces (Figure 3) that may create problems when the candidate surface is analysed to decide if it is a polyp or a fold. To eliminate these undesired surface points from the initial cluster, a *Candidate Surface Processing* procedure is applied. This procedure is described in detail in the next section.

3.2.4   Candidate Surface Processing

To remove the non-convex surface points and the disjoint points from the initial cluster, we developed a Candidate Surface Processing procedure that calculates the Gaussian mapping for each cluster and performs a non-convex surface voxel removal test.

1. *Gaussian Center and Radius Detection*: To calculate the center and radius of each cluster, a Gaussian distribution depicted in Eq. 3 was calculated for

7

each HP of the cluster,

$$GM_i = \sum_{j=1}^{N} e^{(-x^2/2.0 \times \sigma)} \tag{3}$$

where the variable x is the distance between the HPs, σ is the standard deviation and is set to 1. The quantity N is the number of HPs in the cluster and j takes values between $1...N$.

The HP with the highest Gaussian distribution was set as the center of the clustered surface and the Euclidian distance between the center and its corresponding surface point is the radius of the cluster.

2. *Surface Convexity Test*: Let S be a surface voxel, n be the normal vector at the surface voxel S and Q be the intersection point of the surface normal and the perpendicular line from the center of the cluster to the surface normal (see Figure 4). To remove the non-convex points from the initial cluster we employed a simple surface convexity test. In this regard, the non-convex surface point S will be removed from the cluster if the dot product $< \overline{SQ}, \overline{n} >$ is less than zero. In Figure 4, the points *s1* and *s4* and their associated HP will be removed from the cluster as they do not pass the convexity test. We also check the normal distance from the center of the cluster (CP) to the surface normal at position SP and the distance between the surface point (SP) and the intersection point (IP) as illustrated in Figure 5. If the distance between the surface point SP and the intersection point IP is larger than 10mm (the maximum HP distance), the surface point SP is eliminated from the candidate surface.

After the removal of the non-convex surface voxels, each cluster was further processed to evaluate discontinuities in the surface under examination. If dis-

continuities exist in the surface area, the cluster is divided into multiple clusters and their Gaussian maps, centers and radius are recalculated (see Figure 6).

4   Feature Extraction

Our aim is to calculate the features associated with each cluster surface, which will be considered as input for the classifier. The features must be selected in order to maximize the discriminative power between polyps and folds. Recall that the nominal model for polyp is either spherical or ellipsoidal, while the nominal model for fold is cylindrical [19,23]. The features we compute are: Gaussian distribution, sphere fitting error and radius, three axis of the ellipsoid, ellipsoid fit error.

The Gaussian distribution employed to estimate the center and radius of each cluster was calculated in the candidate surface processing stage(see Section 3.2.4). Sphere fitting for each cluster was performed in two phases. Firstly, the error in the least square sphere fitting [33,34] was calculated using the existing Gaussian center and the Gaussian radius of the cluster. Secondly, the cluster radius and the center point were re-calculated using a least square sphere fitting algorithm [33,34]. Experimental results indicate that for spherical polyps, the Gaussian radius and the cluster center were very close to those obtained using the least square estimated sphere and as a consequence the error in fitting is small. For folds the least square estimated radius is higher than the Gaussian radius and the sphere fitting error is significantly higher than the fitting error for polyps. This is illustrated in Figure 7 (note that the polyp and fold classes are ordered by size in ascending order) where the sphere

9

fitting error for a large variety of polyps and folds is plotted.

The principal axes of the fitted ellipsoid and its associated estimation error [33,34] were calculated for each polyp candidate surface and its derived half-radius surface. The half-radius surface voxels are determined from the existing cluster and include those surface voxels which have a distance from the center of cluster to the surface normal less than a *half radius threshold* (HRT). The *HRT* is selected in conjunction with the Gaussian distribution value and varies from 2mm for small cluster surfaces to 5mm for large cluster surfaces. The minimum value of *HRT* (2mm) was experimentally selected. The *Surface Change Rate* (SCR) value computed using Eq. 4 is minimal for polyps (see Figure 8) but it is large for fold (see Figure 9, 10),

$$SCR = (N_T - N_H)/N_H \qquad (4)$$

where N_T is the number of surface voxels in the cluster and N_H is the number of surface voxels in the half radius surface.

It was also found that the change in the major axis direction of the fitted ellipsoid for the candidate surface and the half radius surface was significantly higher for folds when compared to polyps (see Figure 11).

The other features that are used for classifying the candidate surface as polyps and folds are the sphere radius, change in sphere radius, principle axes of ellipsoid fitting, change in ellipsoid fitting error, change in Gaussian distribution. All the above mentioned features exhibit high discrimination between polyps and folds as shown in Figures 7,8, and 11 and these features are employed for polyp detection by our *CAD-CTC* system.

5 Classification

For polyp/fold classification we employed two classifiers, namely the multiple-class-segregated *feature normalized nearest neighborhood* (FNNN) classifier detailed in [35] and *Probabilistic Neural Network* (PNN) [36] in order to evaluate their performance with respect to the detection of true polyps and the reduction of false positive in CAD-CTC. The *FNNN* classification scheme consists of two stages. Firstly, the training database is created by using the features detailed in the previous section for each class of polyps and folds. Features of each class were normalized in order to avoid the situations where the features with the largest values subdue the remaining ones. The feature normalization scheme was performed in order to normalize each feature to zero mean and unit variance as illustrated in Eq. (5) and (6),

$$m_i = \frac{\sum_{j=1}^{k} x_j[i]}{k} \qquad s_i = \sqrt{\frac{\sum_{j=1}^{k} (x_j[i] - m_i)^2}{k}} \qquad (5)$$

$$X_j[i] = \frac{x_j[i] - m_i}{s_i} \qquad for \quad j = 1, ..., k, \quad i = 1, ..., n \qquad (6)$$

where n defines the number of features per pattern, m_i and s_i are the mean and the variance of the ith features, x_j is the unprocessed jth pattern, k defines the number of patterns contained in the model database and X_j represents the normalized jth pattern. The classification stage computes the Euclidian distance between the input objects and the objects contained in the database,

$$dist_j = \sqrt{\sum_{i=1}^{n} (X_j[i] - Y[i])^2} \qquad for \quad i = 1, ..., n \qquad (7)$$

where X_j is the jth object from the model database and Y defines the input pattern to be classified. The input is declared as polyp if the $\min(dist_j)$ belongs

to polyp class, otherwise declared as fold.

Our *FNNN* training databases consist of five polyps and five folds databases. We classify the polyps into small spherical, medium spherical, big spherical, elliptical, and non-spherical polyp. We also divided the fold database into small folds, small convex non-polyp surface, medium folds, large folds, tube. In Figures 7,8 and 11 *class_1 polyp, class_2 polyp, class_3 polyp* and *class_4 polyp* represents small, medium, large and elliptical polyps respectively and *class_1 fold, class_2 fold, class_3 fold* and *class_4 fold* represents large folds, medium size folds, small folds and small convex non polyp surfaces. *Class_5 polyp* and *class_5 fold* in Figures 8 and 11 represent non spherical polyps and surfaces associated with inserted tubes respectively. In total 64 polyps and 155 folds were used to train the *FNNN* and *PNN* classifiers. In our opinion the approach of segregation in polyp training by size offered the optimal solution to increase the polyp identification rate especially for small polyps ($< 5mm$) but not at the expense of increasing the level of false positives.

6   Results

Five patients' data with 33 synthetic polyps [37], 32 patients' data with 101 polyps, and a phantom data with 47 polyps of various sizes [38] were tested using the proposed method. The synthetic polyp insertion in patient data was semi-automatic. The candidate points were manually selected using a custom GUI and the local colon tissue density and the orientation information of the candidate points were used to generate synthetic polyps based on an elliptical model [37]. The overall sensitivity of our *CAD-CTC* system was 90.909% and the false positive level was 3.6 per dataset when the polyp detection

algorithm was applied to synthetic data (Table 1). The sensitivity for polyps greater than 5mm was 100.00% and the sensitivity for polyps less or equal to 5mm was 66.66%. When the algorithm was applied to real databases, the overall sensitivity was 76.24% and the level of false positives per dataset was 4.5 (Table 2). The sensitivity for polyps $>= 10mm$ was 100%, for polyps $[5$ to $10mm)$ was 91.67% and for polyps $< 5mm$ was 69.86%.

The synthetic phantom was constructed using a PVC tube, two acrylic tubes, two plastic plates and latex material to emulate the colon wall and the polyps as depicted in Figure 12 [38]. The polyp inserts for phantom were made using latex material having a HU value of -95. We have chosen to use latex as this material allows us to generate very realistic shapes (pedunculated, sessile, flat, flat-depressed) for polyps as illustrated in Figure 13. The phantom was scanned at 100mAs, 40mAs, 30mAs, and 13mAs with slice thickness of 3mm, reconstruction interval of 1.5mm, table speed of 30mm/rotation, 1.5×16mm collimation and 120kVp. For 100mAs phantom data, the overall sensitivity was 87.23% (Table 3). The sensitivities for polyps $< 5mm$, $[5$ to $10mm)$, $>= 10mm$ and flat polyps were 80%, 100%, 100% and 44.44% respectively (Table 3). The phantom was also scanned at 40mAs, 30mAs, and 13mAs. The overall sensitivities for 40mAs, 30mAs, 20mAs and 20mAs phantom data were 87.23%, 82.97%, 87.23%, 82.97% respectively. The sensitivities for polyps $>= 10mm$ were 100%, 92.95%, 100% and 92.97% when the algorithm was applied to 40mAs, 30mAs, 20mAs and 13mAs phantom data (Tables 4, 5, 6 and 7). The sensitivity for polyps $[5$ to $10mm)$ was 100% in 40mAs, 20mAs, 13mAs phantom data and was 94.73% in 30mAs phantom data. For comparative testing purposes we made the phantom data available from the following web page: $http : //www.eeng.dcu.ie/ \sim whelanp/cadctc$

We also employed a *PNN* classifier to classify candidate surfaces as polyps or folds. Results of the *PNN* classifier are shown in Tables 1 to 7 and clearly demonstrate that our *FNN* classifier outperforms the *PNN* classifier in both sensitivity and false positive reduction.

To determine whether a polyp was correctly detected by the proposed algorithm, we compared the polyp location with the *CTC* reports performed by the radiologists. Also we compared the location of the polyps with the colonoscopy reports. In our tests, we used both supine and prone views for polyp detection. It is important to mention that approximately 20% of the polyps were seen in only one view and as a consequence there was only one chance to detect these polyps.

As indicated in Section 2 the average size of a typical CT dataset was 150MB for each view. The average time required for processing each volume of data was approximately 2.20 min on a Pentium-IV 2.2 GHz processor machine with 512MB memory.

7 Discussion and Conclusion

The proposed CAD system for colonic polyp detection provides high sensitivity for medium and large polyps, while maintaining a low false positive incidence per dataset. Also in our experiments we evaluated two different classifiers in order to determine the optimal classification scheme that minimizes the false positive incidence while keeping the sensitivity higher than 90% for polyps larger than 5mm. Our detection technique shows a relative low sensitivity for small polyps (69.86%). Since we use data with 3mm collimation and 1.5mm

reconstruction interval, the number of surface voxels that belong to polyps less than 5mm is small, and this is the reason why the sensitivity for small polyps is drastically reduced. Another reason for missing small polyps was the condition where the polyp was adjacent to a fold. Therefore, the features derived from small polyps when positioned adjacent to folds show similar characteristics as generic folds, and the classifier detected them as folds. When the *CAD* system was applied to real datasets, 18.18% (4 out of 22) of the undetected small polyps were placed adjacently to folds and the classifier failed to identify them correctly. However, a better surface detection technique in line with an improved reconstruction interval can increase the polyp detection rate when small polyps are situated adjacently to folds.

By using surface normal intersection and least square fitting [33,34] (sphere and ellipsoid) surface features, we tried to obtain the best result from geometrical and statistical methods. In fact, sphere and ellipsoid fitting of surface voxels and circle fitting on three views of the *HPs* may provide good discrimination when the polyps are situated adjacent to folds.

Our developed *CAD-CTC* method presents better results for the detection of small and medium size polyps when applied to lower resolution data (reconstruction interval (RI) 1.5mm) compared to the high resolution *CT* data used to evaluate the methods developed by Kiss et al. [22] (0.8mm RI), Summers et al. [15] (1.0mm RI), Acar et al. [26] (1.0-1.50mm RI), and Kiraly et al. [29] (1.0mm RI). The experimental data indicates that our polyp detection technique also outperforms the methods reported in [13-29] especially when dealing with small and medium sized polyps. Also it is worth mentioning that our algorithm exhibits a remarkable robustness to noise. To demonstrate this, we have applied our algorithm to low-dose phantom datasets (clinical inves-

tigations in Ireland typically use 100mAs as a standard dose) and numerical results are depicted in Tables 4 to 7.

One particular advantage of our method is its low computational overhead and more importantly it shows high sensitivity for medium $[5 - 10mm)$ and large $(\geq 10mm)$ polyps while the false positive rate is maintained at low levels. The experimental results indicate that our CAD polyp detection technique is a suitable tool to be utilised in clinical studies.

Acknowledgments

References

[1] Parker S, Tong T, Bolden S, Wingo P. Cancer statistics 1997. A Cancer Journal for Clinicians 1997;47:5-27.

[2] NCRI, Cancer in Ireland, 1997: Incidence and mortality. Healy & Associates, 2000.

[3] Cancer Research UK. Bowel cancer factsheet - April 2003.

[4] David FR, Robert SS. Screening for colorectal cancer. The New England Journal of Medicine, January 3, 2002;346(1).

[5] American Cancer Society. Cancer facts and figures, 1999.

[6]   National Cancer Institute. Working guidelines for early cancer detection: Rationale and supporting evidence to decrease mortality. Bethesda: National Cancer Institute, 1987.

[7]   Smith RA, Cokkinides V, and Eyre HJ. American cancer society guidelines for the early detection of cancer, 2003 A Cancer Journal for Clinicians 2003;53:27-43.

[8]   Vining DJ, Gelfand DW, Bechtold RE. Technical feasibility of colon imaging with helical CT and virtual reality. American Journal of Roentgenology 1994;162:104.

[9]   Johnson CD, Hara AK, Reed JE. Virtual endoscopy: what's in a name? American Journal of Roentgenology 1998;171:1201-2.

[10] Lichan H, Arie K, YiChih W, Ajay V, Mark W, Zhengrong L. 3D virtual colonoscopy. Proceedings of the 1995 Biomedical Visualization, 30 Oct.-3 Nov. 1995;26-32.

[11] Hara AK, Johnson CD, Reed JE, Ahlquist DA, Nelson H., Ehman RL. Detection of colorectal polyps by CT colonography: Feasibility of a novel technique. Gastroenterology 1996;100:284-290.

[12] Johnson CD, Hara AK. CT colonography: the next colon screening examination? Radiology 2000;216:331-341.

[13] Vining DJ, Hunt GW, Ahn DK, Stelts DR, Helmer PF. Computer-assisted detection of colon polyps and masses. Radiology 1997;205:705.

[14] Summers RM, Johnson CD, Pusanik LM, Malley JD, Youssef AM, Reed JE. Automated polyp detection at CT colonography: Feasibility assessment in a human population. Radiology 2001;219:51-59.

[15] Summers RM, Beaulieu CF, Pusanik LM, Malley JD, Jeffrey RB, Glazer DI,

and Napel S. Automated polyp detector for CT colonography: Feasibility study. Radiology 2000;216:284-290.

[16] Yoshida H, Nappi J. Three-Dimensional computer-aided diagnosis scheme for detection of colonic polyps. IEEE Transactions on Medical Imaging 2001;20(12):1261-1274.

[17] Yoshida H, Masutani Y, MacEneaney P, Rubin DT, Dachman AH. Computerized detection of colonic polyps at CT colonography on the basis of volumetric features: Pilot study. Radiology 2002;222:327-336.

[18] Paik DS, Beaulieu CF, Rey RBJ. Computer aided detection of polyps in CT colonography: Method and free-response ROC evaluation of performance. Radiology 2000;217(P):370.

[19] Kiss G, Cleynenbreugel J, Thomeer M, Suetens P, Marchal G. Computer-aided diagnosis in virtual colonography via combination of surface normal and sphere fitting methods. European Radiology 2002;12(1):77-81.

[20] Kiss G, Cleynenbreugel J, Thomeer M, Suetens P, Marchal G. Computer aided diagnosis for virtual colonography. Medical Image Computing and Computer-Assisted Intervention 2001; 621-628.

[21] Kiss G, Cleynenbreugel J, Thomeer M, Suetens P, Marchal G. Computer aided detection of colonic polyps via geometric feature classication. Vision, Modeling, and Visualization 2002;27-34.

[22] Kiss G, Cleynenbreugel J, Suetens P, Marchal G. Computer aided diagnosis for CT colonography via slope density functions, Medical Image Computing and Computer-Assisted Intervention (1) 2003;746-753.

[23] Paik DS, Beaulieu CF, Rubin GD, Acar B, Jeffrey RBJr, Yee J, Dey J, Napel S. Surface normal overlap: A computer-aided detection algorithm with application

to colonic polyps and lung nodules in helical CT. IEEE Transactions on Medical Imaging 2004;23(6):661-75.

[24] Acar B, Napel S, Paik D, Gokturk SB, Tomasi C, Beaulieu CF. Using optical flow fields for polyp detection in virtual colonoscopy. Medical Image Computing and Computer-Assisted Intervention, Utrecht, The Netherlands, 14-17 October 2001.

[25] Gokturk SB, Tomasi C, Acar B, Beaulieu CF, Paik DS, Jeffrey RBJ, Yee J, Napel S. A statistical 3D pattern processing method for computer aided detection of polyps in CT colonography. IEEE Transactions on Medical Imaging 2001;20(12): 1251-1260.

[26] Acar B, Beaulieu CF, Gokturk SB, Tomasi C, Paik DS, Jeffrey RBJr, Yee J, Napel S. Edge displacement field-based classification for improved detection of polyps in CT colonography. IEEE Transactions on Medical Imaging 2002; 21(12): 1461-7.

[27] Wang Z, Li L, Anderson J, Harrington D, Liang Z. Colonic polyp characterization and detection based on both morphological and texture features. International Congress Series 2004;1268:1004-1009.

[28] Jerebko AK, Malley JD, Franaszek M, Summers RM. Multi neural network classification scheme for detection of colonic polyps in CT colonography data sets, Academic Radiology 2003;10(2):154-160.

[29] Kiraly AP, Laks S, Macari M, Geiger B, Bogoni L, Novak CL. A fast method for colon polyp detection in high-resolution CT data. International Congress Series 2004; 1268:983-988.

[30] Gonzalez RC, Woods RE. Digital image processing. Reading MA: Addison-Wesley, 1993.

[31] Sadleir RJT, Whelan PF. Colon centerline calculation for CT colonography using optimised 3D topological thinning. The International Symposium on 3D Data Processing Visualization and Transmission, Padova, Italy, June 19-21, 2002.

[32] Zucker SW, Hummel RA. A three-dimensional edge operator. IEEE Transactions on Pattern Analysis and Machine Intelligence 1981;3(3):324-331.

[33] Schneider P, Eberly DH. Geometric Tools for Computer Graphics. Morgan Kaufmann Publishers, 2003.

[34] Lancaster P and Salkauskas K. Curve and Surface Fitting: An Introduction. London: Academic Press, 1986.

[35] Ghita O, Whelan PF. A bin picking system based on depth from focus, Machine Vision and Application 2003; 13:234-244.

[36] Neural Network Toolbox, www.mathworks.com, 1992-2001.

[37] Sezille N, Sadleir RJT, Whelan PF. Automated synthesis, insertion and detection of polyps for CT colonography. Opto-Ireland - SPIE's Irish Meeting on Optoelectronics, Photonics and Imaging, Galway, September 5th - 6th, 2002.

[38] Chowdhury TA, Whelan PF, Fenlon H, MacMathuna P. Evaluation of radiation dose on automatic polyp detection at CT colonography: Experiments with a synthetic phantom, Association of Physical Scientists in Medicine, 2005 Annual Scientific Meeting, Galway, Ireland.
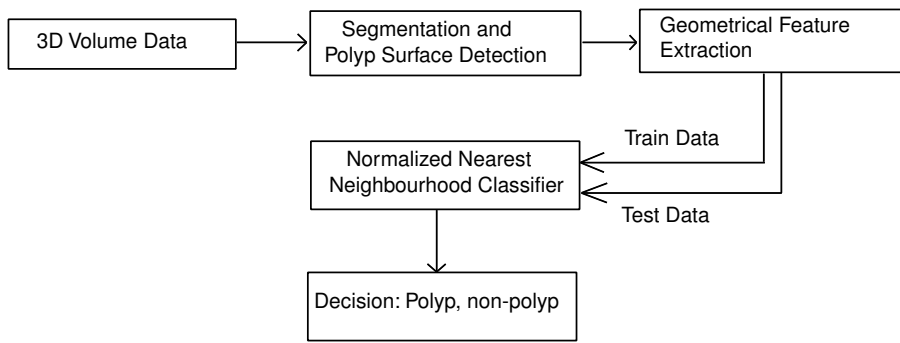
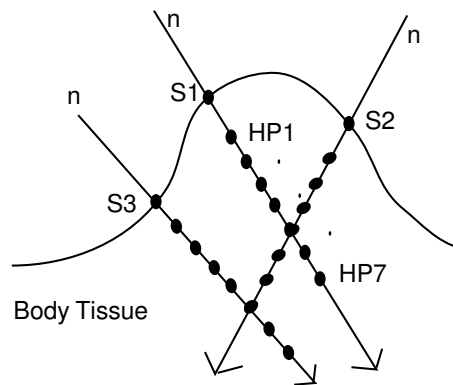Fig. 1. Overview of the proposed CAD-CTC system.

Fig. 2. The distribution of the 7 *Hough Points* (HP) in the normal direction.
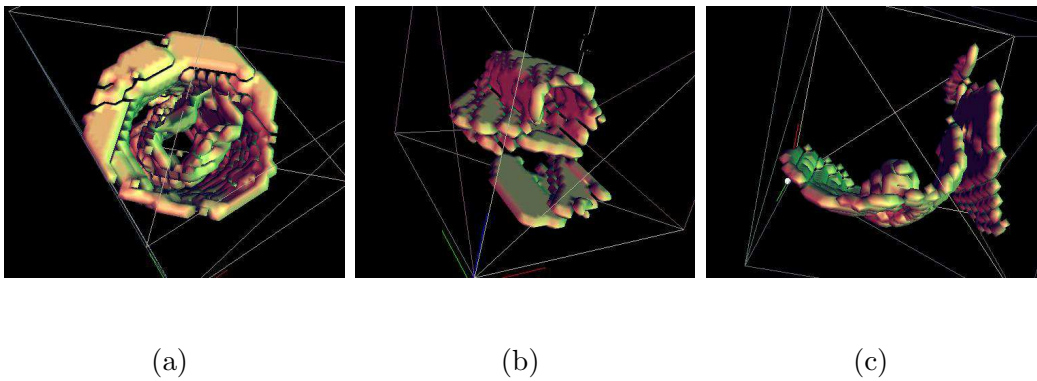
(a)   (b)   (c)

Fig. 3. 3D surface after initial clustering. (a) 3D surface of an inserted tube, (b) 3D surface of a fold and (c) 3D surface of a polyp
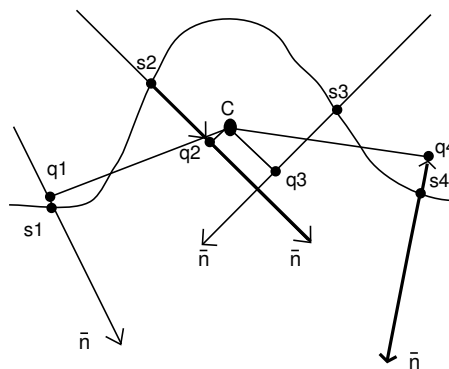

Fig. 4. Convexity test. The point C is the center of the cluster. The surface points $s2$ and $s3$ pass the convexity test whereas the surface points $s1$ and $s4$ and their associated HPs will be removed from cluster as they do not obey the condition that the dot product $< \overline{SQ}, \overline{n} >$ is less than zero.

22
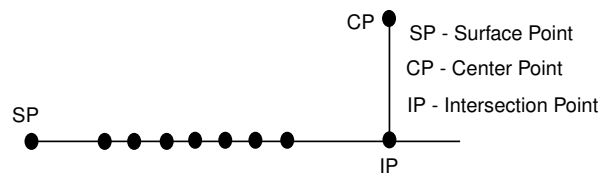
Fig. 5. SP, CP and IP are the surface point, center point and intersection point respectively. Circles between the SP and IP represent the 7 *HPs* for each surface point.
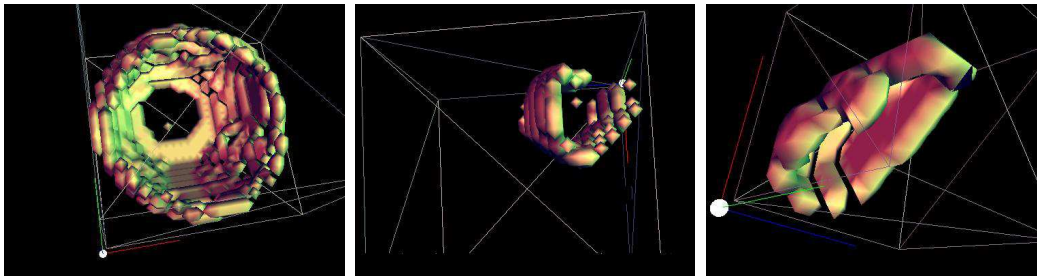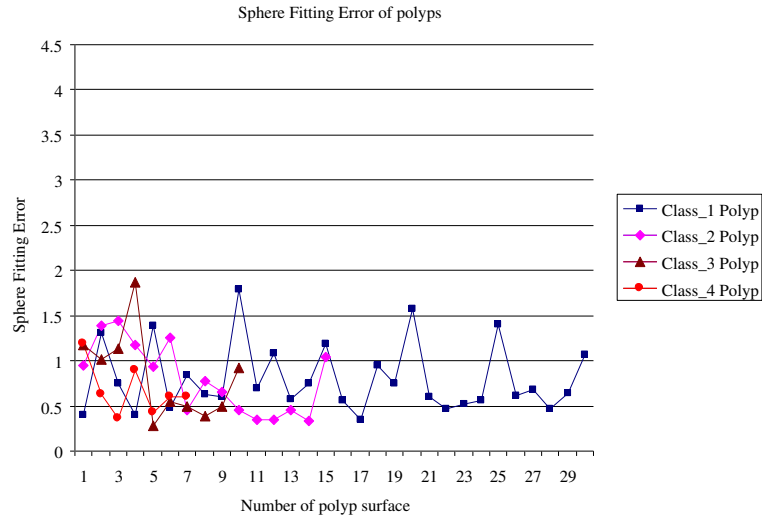

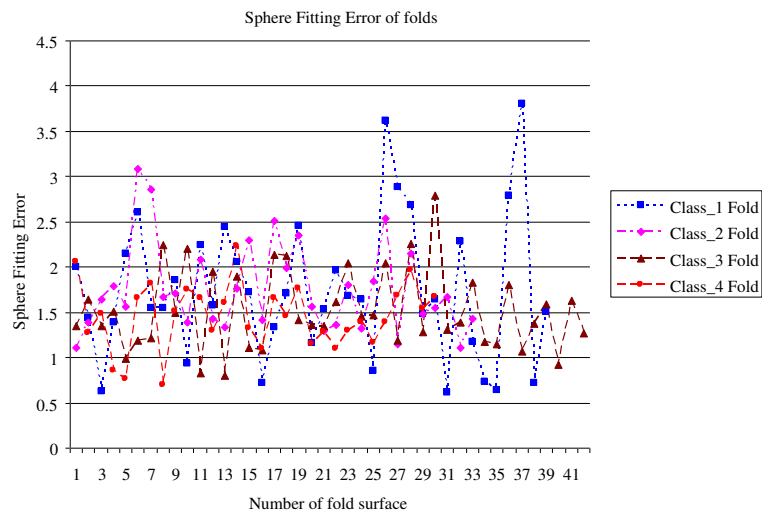(a)   (b)   (c)

Fig. 6. 3D surface after re-clustering the voxels of the candidate surface. (a) 3D surface of the inserted tube illustrated in Figure 3a, (b) 3D surface of the fold illustrated in Figure 3b, (c) 3D surface of the polyp illustrated in Figure 3c.
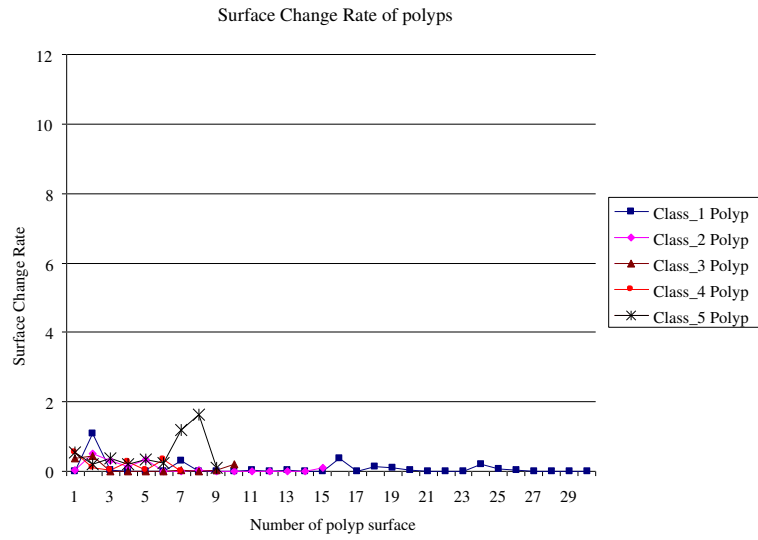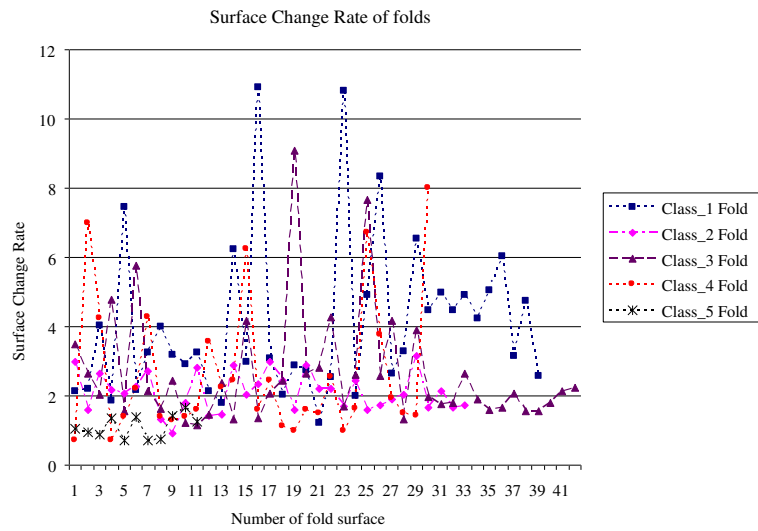
(a)

(b)

Fig. 7. Sphere fitting error analysis. (a) and (b) represent sphere fitting error analysis for different classes of polyps and folds respectively (polyps and folds classes are sorted by size in ascending order).

(a)

(b)

Fig. 8. Surface change rate. (a) and (b) show the surface change rate for different classes of polyps and folds.
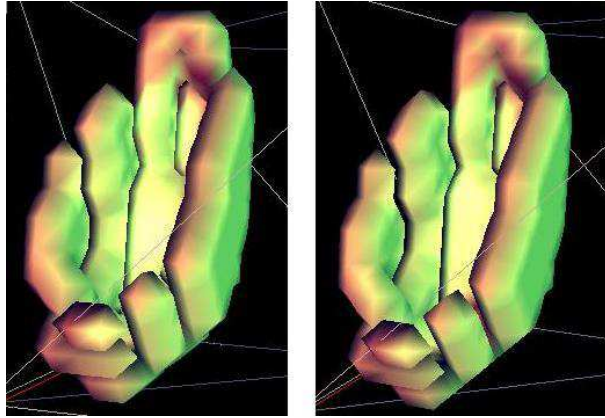
25

Fig. 9. 3D surface generation of a polyp (a) and its half radius surface (b). No significant differences in shape between them are noticed.
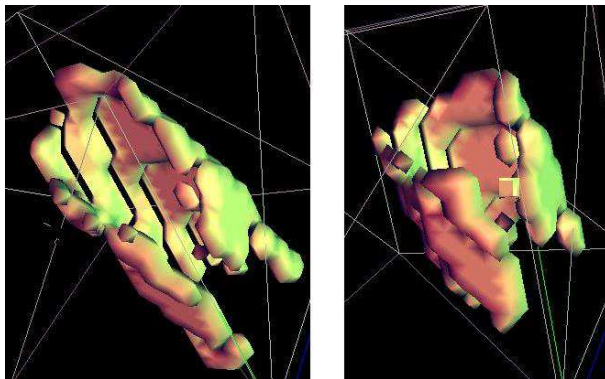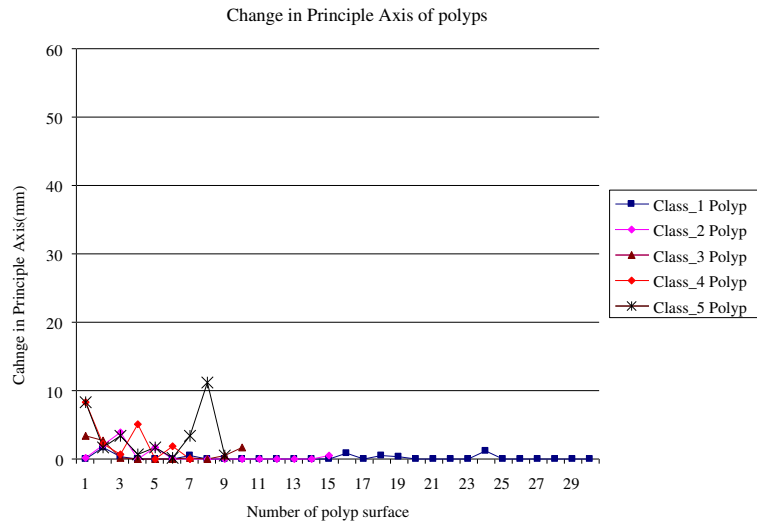

Fig. 10. 3D surface generation of a fold (a) and its half radius surface (b). It can be noticed a significant difference in shape between them.

(a)
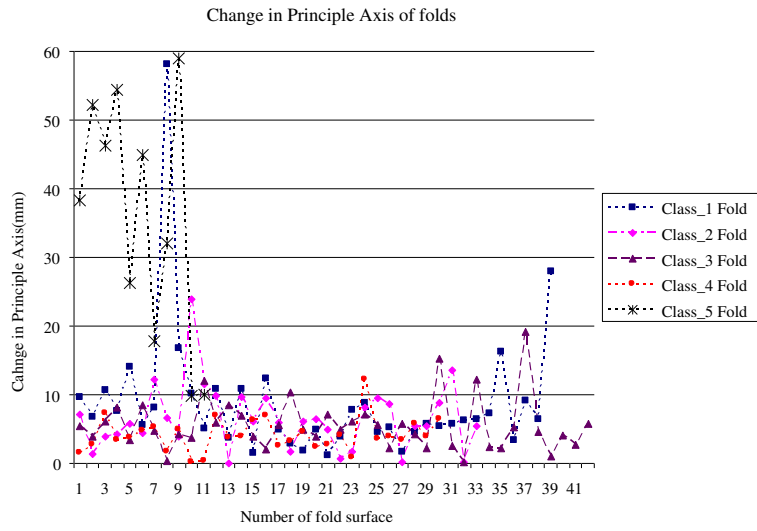
(b)

Fig. 11. Change in major (principle) axis orientation. (a) and (b) display the change in major axis orientation for different classes of polyps and folds.

(a)   (b)

Fig. 12. Synthetic colon phantom. (a) Longitudinal view. (b) Transversal view.

Fig. 13. Latex sheet with various types of phantom polyps and folds.

Table 1
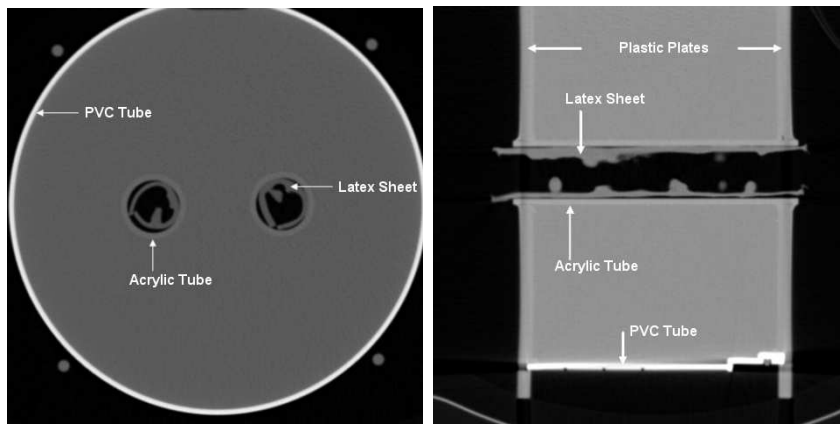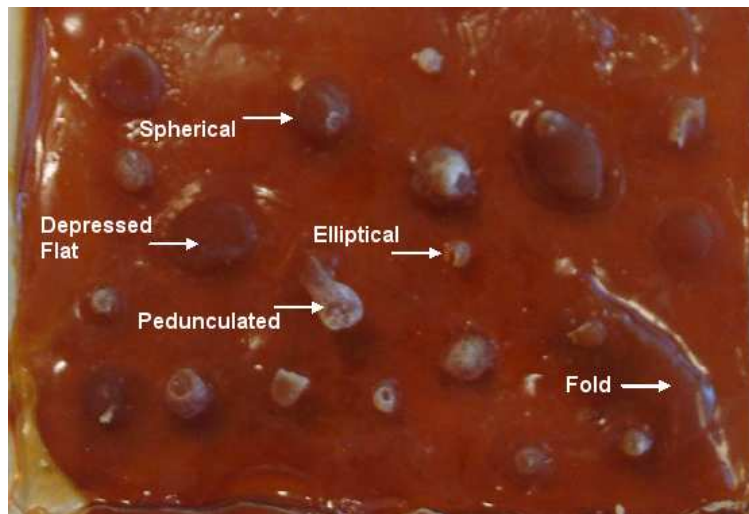
Performance analysis for synthetic polyp data

Type	Number	FNNN		PNN	
		True Positive	*Sensitivity*	*True Positive*	*Sensitivity*
$< 5mm$	6	4	66.66%	2	33.33%
$[5-10)mm$	17	17	100%	15	88.24%
$\geq 10mm$	9	9	100%	7	77.78%
Flat	1	0	00.00%	0	0%
Total	33	30	90.91%	24	72.73%
FP			3.6		6.4

Table 2

Performance analysis for real polyp data

Type	Number	FNNN		PNN	
		True Positive	*Sensitivity*	*True Positive*	*Sensitivity*
$< 5mm$	73	51	69.86%	48	65.75%
$[5-10)mm$	24	22	91.67%	17	70.83%
$\geq 10mm$	4	4	100%	3	75%
Flat	2	1	50%	1	50%
Total	103	78	75.73%	69	66.99%
FP			4.54		6.7

Table 3

Performance analysis for phantom polyp data

Type	Number	FNNN		PNN	
		True Positive	*Sensitivity*	*True Positive*	*Sensitivity*
< 5mm	5	4	80%	3	60%
[5 − 10)mm	19	19	100%	18	94.74%
≥ 10mm	14	14	100%	13	92.86%
Flat	9	4	44.44%	2	22.22%
Total	47	41	87.23%	36	76.60%
FP			2		2

Table 4

Performance analysis for low-dose (40 mAs) phantom polyp data

mAs	Type	Number	FNNN		PNN	
			True Positive	*Sensitivity*	*True Positive*	*Sensitivity*
40	< 5mm	5	4	80%	3	60%
40	[5 − 10)mm	19	19	100%	18	94.74%
40	≥ 10mm	14	14	100%	14	100%
40	Flat	9	4	44.44%	1	11.11%
Total		47	41	87.23%	36	76.60%
FP				3		4

Table 5

Performance analysis for low-dose (30mAs) phantom polyp data

mAs	Type	Number	FNNN		PNN	
			True Positive	*Sensitivity*	*True Positive*	*Sensitivity*
30	< 5mm	5	4	80%	3	60%
30	[5 − 10)mm	19	18	94.74%	15	78.94%
30	≥ 10mm	14	13	92.86%	12	85.71%
30	Flat	9	4	44.44%	1	11.11%
Total		47	39	82.98%	31	65.96%
FP				4		4

Table 6

Performance analysis for low-dose (20mAs) phantom polyp data

mAs	Type	Number	FNNN		PNN	
			True Positive	*Sensitivity*	*True Positive*	*Sensitivity*
20	< 5mm	5	4	80%	3	60%
20	[5 − 10)mm	19	19	100%	16	84.21%
20	≥ 10mm	14	14	100%	12	85.71%
20	Flat	9	4	44.44%	2	22.22%
Total		47	41	87.23	33	70.21%
FP				4		2

Table 7

Performance analysis for low-dose (13mAs) phantom polyp data

mAs	Type	Number	FNNN		PNN	
			True Positive	*Sensitivity*	*True Positive*	*Sensitivity*
13	$< 5mm$	5	4	80%	3	60%
13	$[5-10)mm$	19	19	100%	17	89.47%
13	$\geq 10mm$	14	13	92.85%	12	85.71%
13	Flat	9	3	33.33%	2	22.22%
Total		47	39	82.98%	34	72.34%
FP				3		4